Inspection of Imprint Lithography Patterns for Semiconductor and Patterned Media

Douglas J. Resnick, Gaddi Haase, Lovejeet Singh, David Curran, Gerard M. Schmid, Kang Luo, Cindy Brooks, Kosta Selinidis, John Fretwell, S.V. Sreenivasan
Molecular Imprints Inc. 1807-C W. Braker Lane Austin, TX 78758, USA

Abstract

Imprint lithography has been shown to be an effective technique for replication of nano-scale features. Acceptance of imprint lithography for manufacturing will require demonstration that it can attain defect levels commensurate with the requirements of cost-effective device production. This work summarizes the results of defect inspections of semiconductor masks, wafers and hard disks patterned using Jet and Flash Imprint Lithography (J-FIL™). Inspections were performed with optical and e-beam based automated inspection tools.

For the semiconductor market, a test mask was designed which included dense features (with half pitches ranging between 32 nm and 48 nm) containing an extensive array of programmed defects. For this work, both e-beam inspection and optical inspection were used to detect both random defects and the programmed defects. Analytical SEMs were then used to review the defects detected by the inspection. Defect trends over the course of many wafers were observed with another test mask using a KLA-T 2132 optical inspection tool. The primary source of defects over 2000 imprints were particle related.

For the hard drive market, it is important to understand the defectivity of both the template and the imprinted disk. This work presents a methodology for automated pattern inspection and defect classification for imprint-patterned media. Candela CS20 and 6120 tools from KLA-Tencor map the optical properties of the disk surface, producing high-resolution grayscale images of surface reflectivity, scattered light, phase shift, etc. Defects that have been identified in this manner are further characterized according to the morphology

Keywords: jet and flash imprint lithography, J-FIL, imprint lithography, imprint mask, template, defectivity, optical inspection, electron beam inspection

1. Introduction

Imprint lithography has been shown to be an effective technique for replication of nano-scale features. When the imprint material is a photocurable liquid, it is possible to perform the patterning process at low temperature and ambient pressure, which enables accurate overlay and reduces process defectivity. The resolution of the imprint approach is strictly dependent on the ability to create a 1X master mask or template, and improvements in resolution can be achieved without new optical systems or photoresist materials. In this sense, imprint lithography is a multi-generational technique that is being used to facilitate device and process prototyping at several upcoming lithography nodes.

Acceptance of imprint lithography for manufacturing will require demonstration that it can attain defect levels commensurate with the requirements of cost-effective device production. This work summarizes the results of defect inspections of semiconductor masks, wafers and hard disks patterned using Jet and Flash Imprint Lithography (J-FIL™)[1-7]. Inspections were performed with optical and e-beam based automated inspection tools.

For the semiconductor market, it will be necessary to detect defects less than the half pitch of the device. A test mask was designed which included dense features (with half pitches ranging between 32 nm and 48 nm) containing an extensive array of programmed defects. For this work, both e-beam inspection and optical inspection were used to detect both random defects and the programmed defects. Analytical SEMs were then used to review the defects detected by the inspection. Defect trends over the course of many wafers were observed with another test mask using a KLA-T 2132 optical inspection tool. The primary source of defects over 2000 imprints were particle related.

For the hard drive market, it is important to understand the defectivity of both the template and the imprinted disk. This work presents a methodology for automated pattern inspection and defect classification for imprint-patterned media. Candela CS20 and 6120 tools from KLA-Tencor map the optical properties of the disk surface, producing high-resolution grayscale images of surface reflectivity, scattered light, phase shift, etc. We have developed software that

Alternative Lithographic Technologies II, edited by Daniel J. C. Herr, Proc. of SPIE Vol. 7637
76370R · © 2010 SPIE · CCC code: 0277-786X/10/$18 · doi: 10.1117/12.848391

Downloaded from SPIE Digital Library on 23 Nov 2011 to 216.110.75.11. Terms of Use: http://spiedl.org/terms

analyzes these images and identifies defect pixels distinctly from the pixels that correspond to data storage structures or servo patterns. Defects that have been identified in this manner are further characterized according to the morphology of the defect pixels as well as the defect location on the substrate. Included in this work are the classification of the defects and a defect source analysis for an extended imprint run on disks.

2. Experimental Details

2a. Semiconductor

To generate the inspection test mask, patterns were exposed by Dai Nippon Printing using a JEOL 9300 Gaussian beam pattern generator. ZEP520A resist was chosen as the positive imaging resist. After development, the chromium and fused silica were etched using Cl_2/O_2 and fluorine-based chemistry, respectively. Mesa lithography and a mesa etch process, followed by a dice and polish step were employed to create a finished 65 mm x 65 mm template.[8]

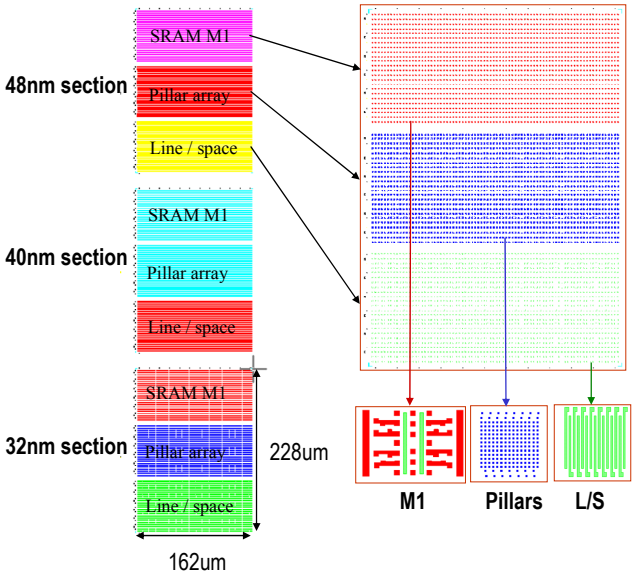

Figure 1. Programmed defect layout

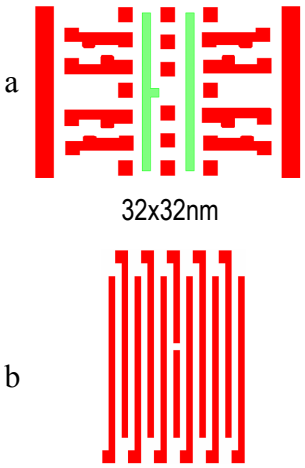

Figure 2. a) Extension defect in the SRAM Metal1 pattern. b) Mousebite in the line/space array.

The pattern chosen for evaluation was a 32 nm half pitch design with several different pattern types. Each pattern, in turn, had an array of programmed defects introduced into the pattern. The details are shown in Figure 1. Three different half pitches were studied: 48 nm, 40 nm and 32 nm. For each size, three pattern types were designed: SRAM Metal 1, pillar array, and a dense line/space pattern. For each feature type, multiple programmed defects were inserted. As an example for the 32nm lines and spaces, twelve incremental programmed sizes were inserted, starting at 4 nm and ending at 48 nm. Extension defects included three repeats in the horizontal and vertical directions , for a total of 72 defects. Mousebites were inserted in the same fashion to create a total of 144 defects. Examples of extension defects for the Metal1 and mousebites in the line/space pattern are shown in Figure 2.

Initial characterization of the imprint mask was done using both a Holon EMU-270A SEM and a KLA-Tencor LWM9045 SEM. The EMU-270A is capable of 1.5 nm resolution at 1.0 kV when applying aberration correction. Low vacuum operation, combined with proprietary charge control enables high quality imaging on uncoated fused silica masks. The KLA-Tencor LWM9045 CD SEM uses proprietary technology to control the charging effect, employs a new electron detector system, and provides stable imaging conditions to avoid image drift. Mask images of the 32nm line/space patterns, including a programmed mousebite defect are shown in Figure 3.

Downloaded from SPIE Digital Library on 23 Nov 2011 to 216.110.75.11. Terms of Use: http://spiedl.org/terms

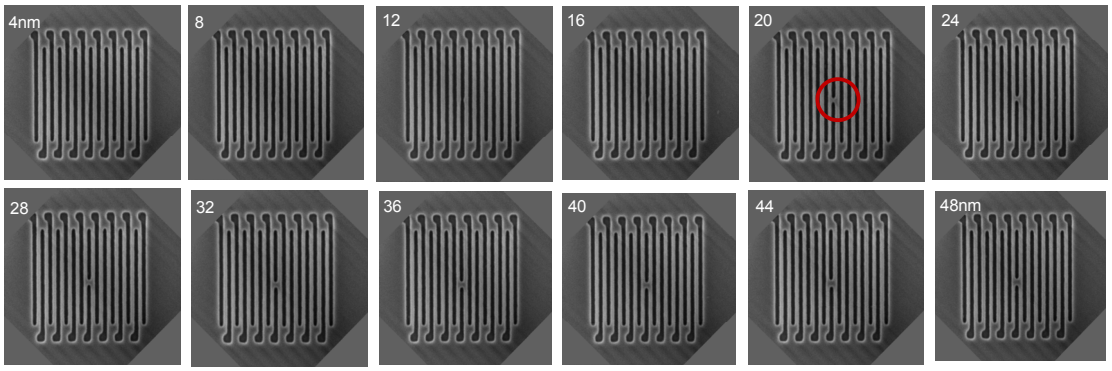

Figure 3. Mask SEM images. Note that the 20nm programmed defect results in a bridged pattern.

Imprinting of the mask pattern was performed by using a Molecular Imprints Imprio® 300 imprint tool. A Drop-On-Demand method was employed to dispense the photo-polymerizable acrylate based imprint solution in field locations across a 300 mm silicon wafer. The template was then lowered into liquid-contact with the substrate, displacing the solution and filling the imprint field. UV irradiation through the backside of the template cured the acrylate monomer. The process was then repeated to completely populate the substrate. Details of the imprint process have previously been reported.[9]

Die-to-die wafer inspection was done with both a KLA-Tencor eS35 and a Hermes Microvision (HMI) eScan 315 electron beam inspection . The eS35 operated at a data rate of 50 megapixels per second, with pixel settings of 15, 20, and 25nm. Landing energy was set to 1750 volts and eight scans were collected. The eScan 315 operated at a data rate of 100 megapixels per second with pixel settings of 10 and 15nm. Landing energy was 2000 volts and eight scans were also collected. Die-to-database inspection was performed using an NGR2100 e-beam wafer system. The data rate was set at 50 megapixels per second, and the landing energy was 2600 volts. Although a 3nm pixel setting was used, the detection threshold was set to 10nm.

Optical inspection of the programmed defect mask was performed on a KLA-Tencor 6xx mask inspection tool operating at a 193nm wavelength, with a smaller pixel than previous generations of tools. Improved image processing is incorporated to provide traditional high-resolution reticle plane inspection for production of advanced masks and reticles. Both transmitted and reflected light modes were used to examine the programmed defects.

A second imprint mask was designed for an extended imprint study (See Figure 4.). The field contained four identical die of SRAM-like metal-1 features with a minimum critical dimension (CD) of 350 nm and 4 die of 400 nm contact features. The field also contains smaller features; metal layer features down to 70 nm and 120 nm contacts. In the center of the pattern a set of program defect features were included and were the focus for defect inspection using a KLA-Tencor 2132 wafer inspection tool. Seventeen wafers containing over 2000 imprinted fields were printed and inspected for repeating defects.

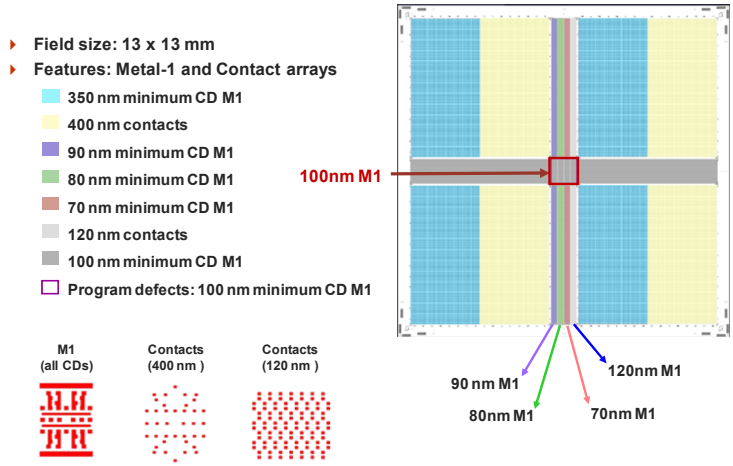

Figure 4. Mask design used to examine printed patterns. In this work, the focus was on the central 100nm Metal1 pattern.

Downloaded from SPIE Digital Library on 23 Nov 2011 to 216.110.75.11. Terms of Use: http://spiedl.org/terms

b. Patterned Media

The replica template used for this study was fabricated from a master template with 120 nm pitch media and an accompanying set of generic servo patterns. The patterns started at an inner radius of 16.5 mm and continued out to a radius of 31.5 mm. Replication of the master was done using an Imprio 100TR system. Pattern transfer of the template was done in an RIE etcher from Trion. The replica mask, discrete tracks and servo patterns are shown in Figure 5.

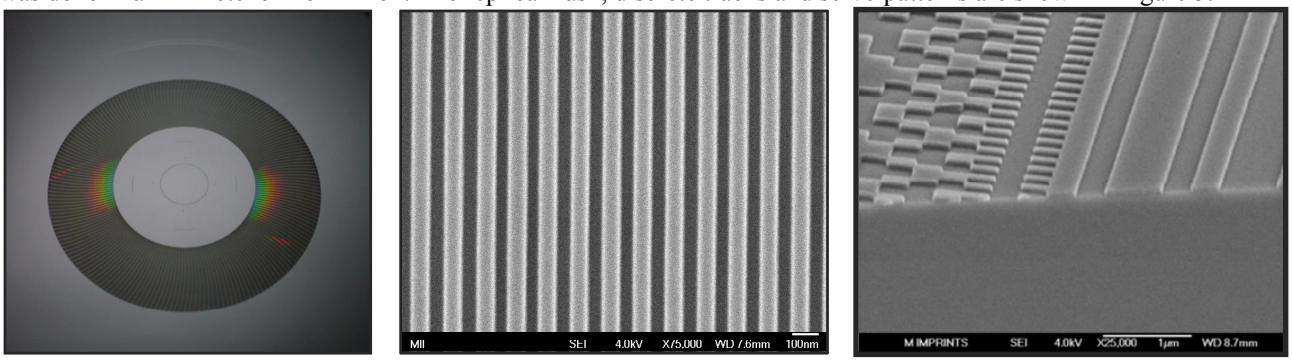

a b c

Figure 5. a) Optical image of the replica template. B) SEM of the discrete tracks. C) SEM of the generic servo patterns.

Two-sided imprinting of disk substrates was performed with an Imprio HD2200 – a fully automated UV nanoimprint lithography tool that has been specifically designed for patterned media applications[10]. The Imprio HD2200 provides the high patterning fidelity that is characteristic of UV-nanoimprint lithography, with automated double-sided disk patterning capability and throughput of 180 disks per hour. Patterned media applications typically require a modest level of alignment (tens of microns) to ensure that the patterns are concentric to the spindle axis of the disk drive unit; the Imprio HD2200 provides alignment of the template pattern to the disk substrate within 10 µm. The next generation system is scheduled for delivery in first quarter of 2010 and will have a throughput greater than 300 disks per hour, double sided.

Inspection on both templates and disks were performed using Candela systems from KLA-Tencor. Candela tools scan the substrate surface under the stationary inspection spot of the X-Beam™ Optical Surface Analyzer. Two high stability laser sources (with adjustable polarization) are directed to this location in radial and circumferential orientations, and multiple detectors are employed to measure the scattered light as well as the intensity and phase of the specular reflection. This flexible configuration permits both bright field and dark field inspection modes as well as quantitative thin film ellipsometry measurements. Originally used for inspection of ultra-thin lubrication layers on unpatterned disk surfaces, these tools are also useful for inspection of the next generation of patterned media. A schematic of the Candela is shown in Figure 5. A typical scan image is shown in Figure 6.

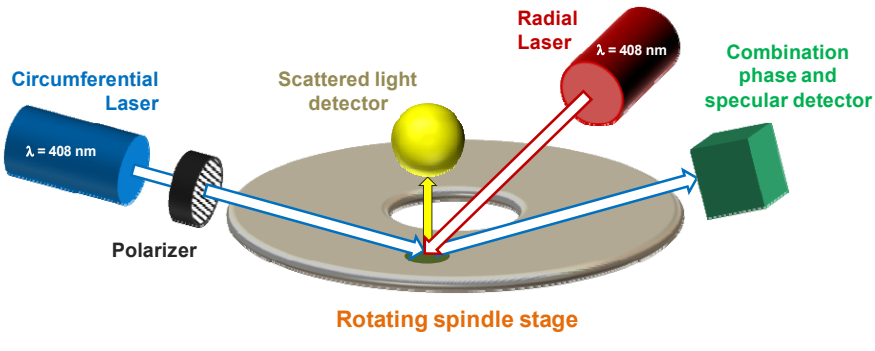

Figure 5. Schematic of optical components in a Candela® inspection tool.

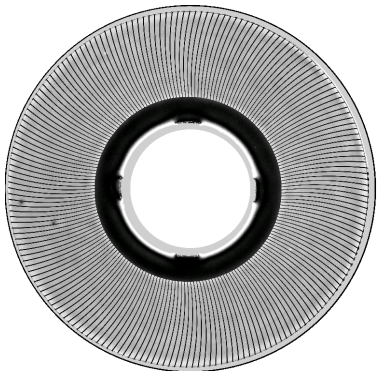

Figure 6. Candela image of a template.

Downloaded from SPIE Digital Library on 23 Nov 2011 to 216.110.75.11. Terms of Use: http://spiedl.org/terms

3. Semiconductor Results

a. E-beam Inspection

The defect size trend for both mask and imprint are shown in Figure 7. Pictured is the trend for the shrinking pillars. Notice the excellent agreement in defect size between the mask and imprint. As the pillar is shrunk to a diameter less than 16 nm, the feature is no longer resolved on the mask, and the defective area jumps in size. The defective area then remains constant until the programmed pillar above the central pillar is also shrunk. The exact same trend is also observed in the line/space patterns. In the case of the line/space array, the discontinuity occurs at 20nm.

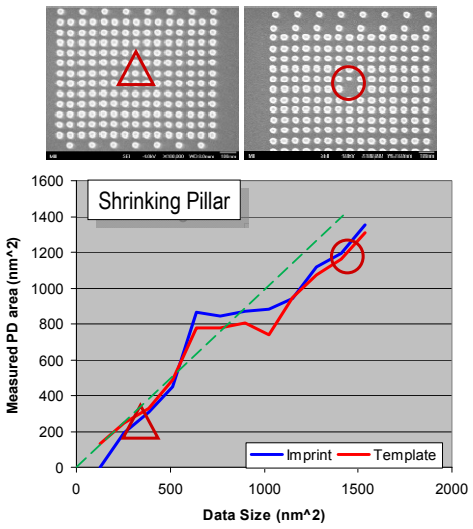

Figure 7. Measured defect size versus coded defect size for the dense pillar array.

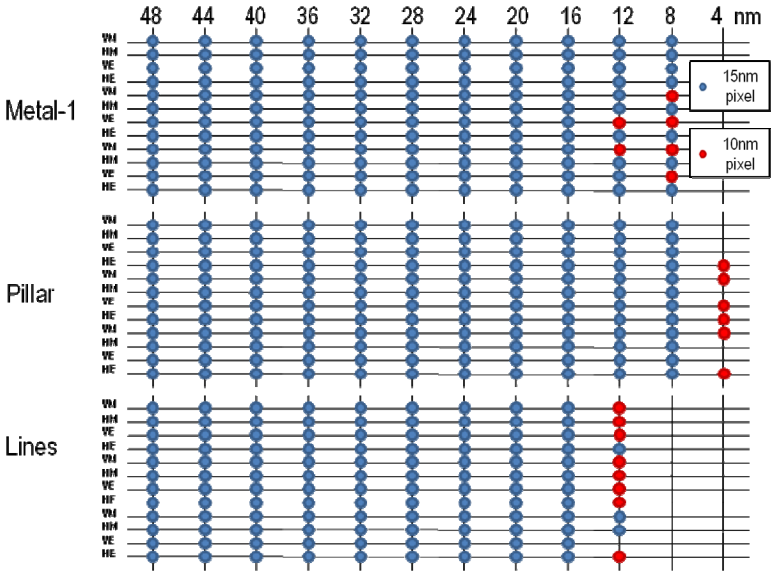

Figure 8. Capture rate as a function of programmed defect size for 15nm and 10nm pixel settings.

Figure 8 shows the inspection results of the 32nm programmed defects using the eScan315. Details for both the eScan inspection and the eS35 inspection have been previously reported[11]. The blue dots in Figure 8 indicate the programmed defects captured at a 15nm pixel setting. All of the 16nm programmed defects were captured, and more than half of the 12nm defects were captured. As in the case of the results from the eS35, the eScan system is most sensitive to changes in the pillars. In fact, at a 15nm pixel setting, all of the 8nm programmed defects are captured. Better results are obtained at the 10nm pixel setting (red cells). All but one of the 12 nm defects are detected, and 67% of the 8nm defects were observed.

a. Optical Mask Inspection

It is anticipated that mask lifetime for an imprint mask will be on the order of 50,000 imprints. As a result, a mask replication strategy is being employed to address mask lifetime. With respect to mask inspection, a master mask will require a high resolution inspection, such as electron beam inspection. Inspection time for these systems are slow, however, and will not be able to meet the throughput requirements for the many replica masks required. Instead, an optical inspection tool will be needed that still has good resolution, but is able to inspect replica masks in less than one hour.

A KLA-Tencor 6xx optical mask inspection tool was tested, to understand whether defects on the order of the half pitch could be detected. The programmed defect mask described in Section 2a was used for testing purposes. Initial results are promising. This first study focused on the 32nm line/space patterns. Shown in Figure 9 are examples of two

Downloaded from SPIE Digital Library on 23 Nov 2011 to 216.110.75.11. Terms of Use: http://spiedl.org/terms

different defect types inspected in Transmitted (top row) and Reflected (bottom row) light mode. The reference cell is shown in the first column and the programmed defect cell (PD) is shown in the second column. The difference in the images is shown in the final column. Note that although it is not possible to distinguish the individual lines in the pattern, the defect is clearly observed. Note that depending on the defect type, one mode produces a better view of the defect than the other, indicating that both nodes will be necessary to detect different types of defects.

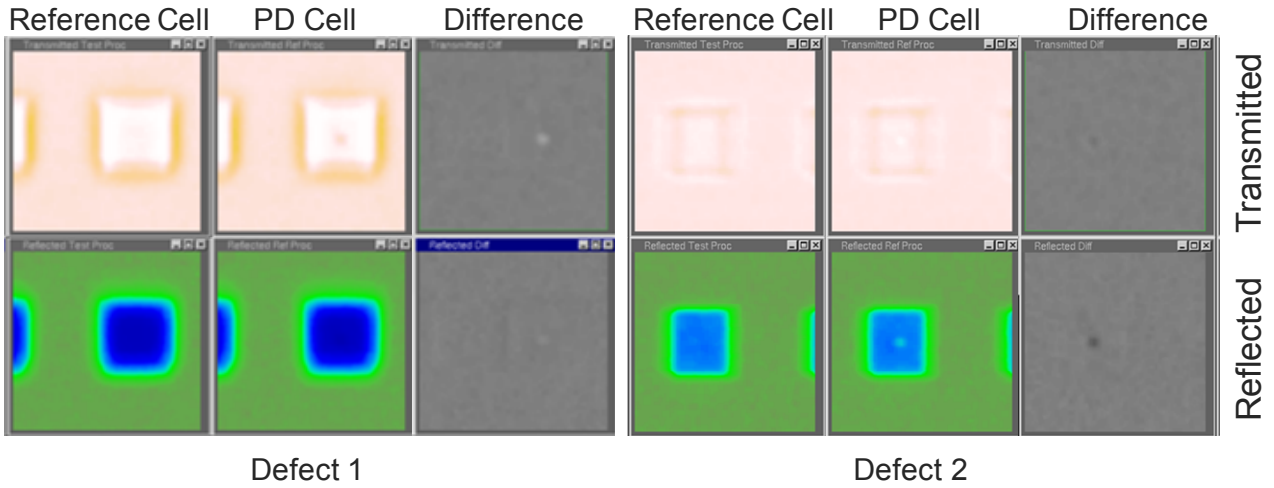

Figure 9. Images of two programmed defects on 32nm half pitch patterns. Left image: Reference cell, Right Image: Programmed defect cell, Right image: Difference

The modulation of the observed defect tracks very well with the actual measured size of the defect, as shown in Figure 10. Figure 10a shows the defect trend described earlier. A linear behavior is observed until a discontinuity occurs where the programmed defect bridges the gap between lines. The measured defect them remains unchanged until the defect is grown in the vertical direction. Figure 10b shows the signal modulation of the detected defect as a function of defect size. Based on the magnitude of the modulation, the smallest detectable defect is on the order of the half pitch. It should be noted that because the patterned background noise is low, it should be possible improve the threshold and detect even smaller defects.

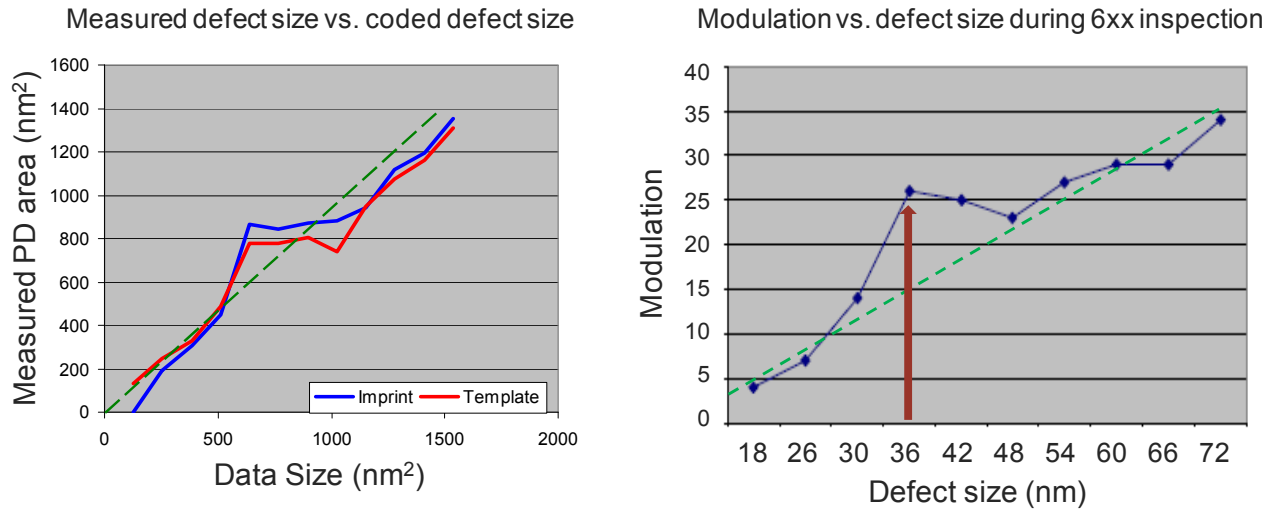

Figure 10. a) Measured programmed defect as a function of data size. Note the non-linear behavior. b) Signal modulation of the KLA-T 6xx. Note the same non-linear response in modulation when compared with Figure 10a.

Downloaded from SPIE Digital Library on 23 Nov 2011 to 216.110.75.11. Terms of Use: http://spiedl.org/terms

c. Wafer Inspection

To understand imprint defectivity, a 2000 imprint run covering 17 wafers was made using the test mask described in Figure 4. Random defectivity with J-FIL is quite low, therefore this study focused on the repeater defects encountered while imprinting.[12] A KLA-Tencor 2132 wafer inspection tool, with sensitivity on the order of 100nm, was used to examine the printed fields. The results are shown in Figure 11. Four repeater defects appeared over the course of the run. Of the four, two defects were "self cleaned", leaving two defects after the end of the run.

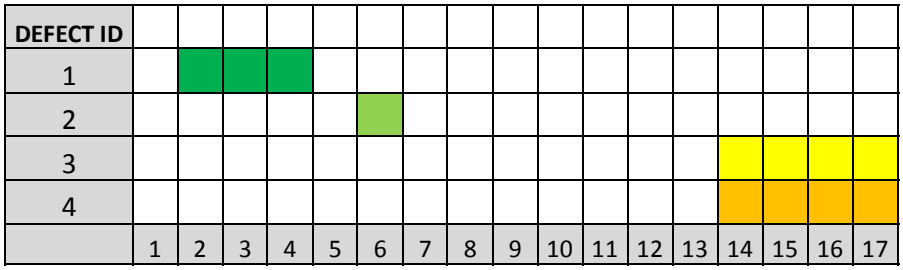

Figure 11. Defects detected over 17 wafers. The majority of the defects found are particle related.

The results for this run are typical of previously reported imprint runs.[12] Two dominant defect types were identified. The majority of the defects are particle related. An example of this defect type is shown below. The defect was first noted on wafer 14. SEM analysis discovered that the source of the defect was a particle on the wafer. The progression of pictures shows the first field where the particle was discovered, three imprints after the particle, and the steady state result on wafer 17. EDX analysis indicated that the particle contained aluminum. This is a relatively rare event; most particle tend to be purely organic.

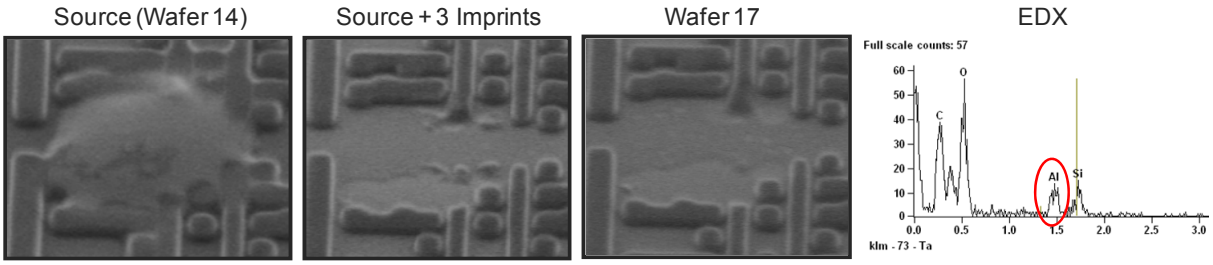

Figure 12. Particle induced defect. Although Al was detected in this particle, the majority of particles are organic.

The second defect type is designated as a plug defect. A plug defect may occur when residual material (including resist) becomes lodged in a mask feature, thereby preventing printing. In the example below, the defect was first detected on wafer 2 in imprint #72. By moving back in imprint sequence, it was observed that the defect was always present in the mask, and slowly grew until it was detectable by the KT2132. The root cause of the mask imperfection is not well understood.

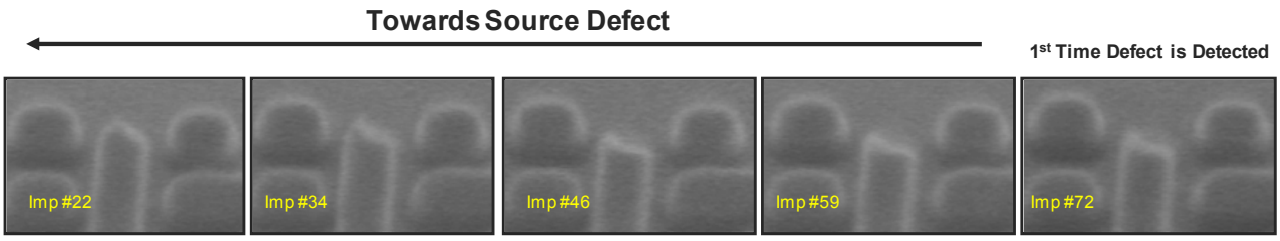

Figure 13. Plug defect caused by an imperfection in the mask.

Downloaded from SPIE Digital Library on 23 Nov 2011 to 216.110.75.11. Terms of Use: http://spiedl.org/terms

4. Patterned Media Results

a. Candela defect characterization

Implementation of PM in production requires pattern inspection at levels of resolution and throughput that are sufficient to obtain meaningful statistics on process yield; this metrology facilitates the feedback loop that is essential for process optimization and control. Fortunately, a disk drive is more tolerant of defects than a typical semiconductor device. For example, a low level of small, isolated defects can reduce the area that is available for data storage, but the overall performance of the disk drive is not affected. This level of defect tolerance can be specified simply in terms of the fraction of the disk surface that is unusable for recording data. However, defects within the servo patterns are more problematic because these defects can impair the function of the drive head. This issue is mitigated through use of fault-tolerant servo pattern designs, but increased fault tolerance requires a larger portion of the disk surface to be devoted to servo marks (at the expense of data storage). The tolerance specifications for lithography defects are thereby tied to a number of other process and design decisions.

The details of the lithography defect specifications (proprietary to each media supplier) will determine the appropriate defect inspection strategy. While details of the defect inspection strategies vary, it is clear that pattern inspection will occur at multiple points during the PM lithography process, beginning with the qualification of templates. As is the case for replica masks, replica templates and patterned disks require short inspection times due to the much larger volume of substrates.

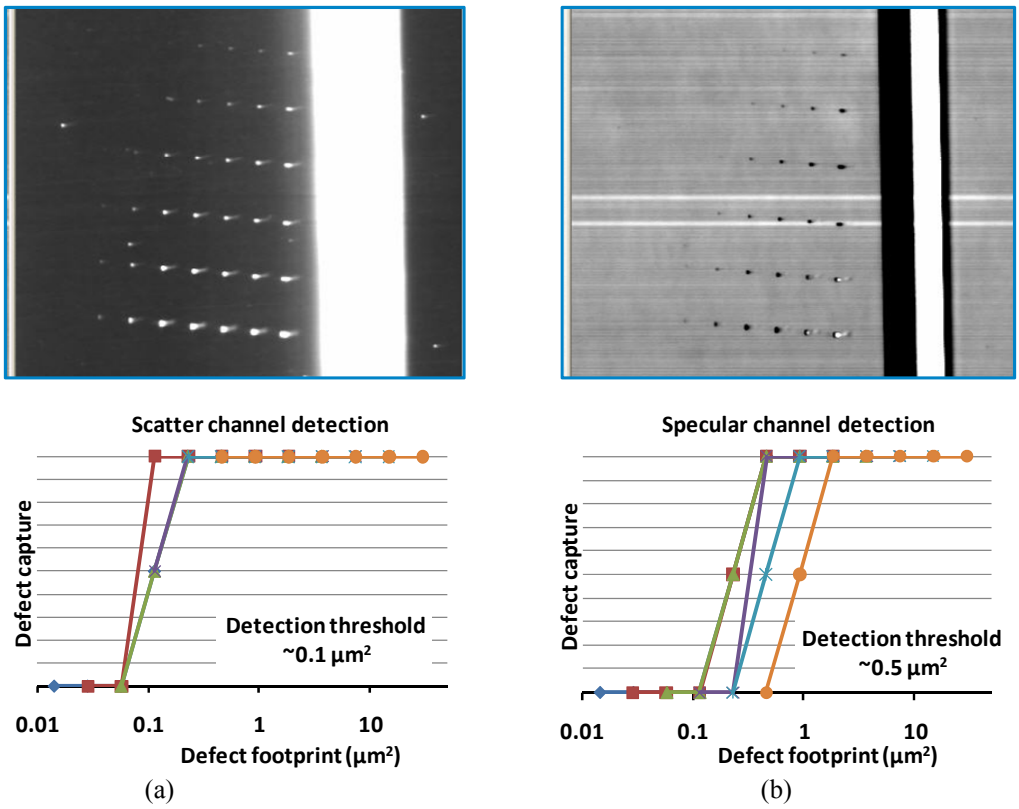

Figure 14. a) Scatter-channel image of a DTR template that includes an array of programmed defects. The captured of programmed defects as a function of the nominal footprint area are shown below the image. b) Specular-channel image along with the captured programmed defects.

Candela inspection systems were used for all inspections. Although the minimum pixel size of the optical system (~1 micron) is much larger than the lithographic patterns, the stability of the optical systems and the availability of

Downloaded from SPIE Digital Library on 23 Nov 2011 to 216.110.75.11. Terms of Use: http://spiedl.org/terms

multiple inspection channels enable detection of sub-200nm pattern defects. To investigate the sensitivity of the Candela tools for detection of small pattern defects, a test template was prepared with arrays of programmed defects embedded within a DTM layout having a track pitch of 120nm. The programmed defect array consisted of rectangles ranging from 0.12 μm to 7.68 μm, with varying aspect ratio in both down-track and cross-track directions. Figures 14a and 14b present Candela scans of an array of programmed defects using the scatter and specular channels, respectively. The corresponding capture efficiencies for programmed defects are plotted below the two images. The scatter channel is found to be more sensitive for capture of small defects, with nearly complete capture of programmed defects having a footprint area of at least 0.1 μm^2. The specular channel is somewhat less sensitive for detection of the smallest programmed defects, with an apparent threshold area of ~0.5 μm^2. However, the specular channel image in Figure 14b reveals pattern details that are not seen in the scatter channel image of Figure 14a. For example, two non-programmed pattern errors are evident as horizontal lines; these errors originated as electron-beam stitching errors. The specular inspection mode also reveals details of the servo patterns that are not seen with a scattering mode inspection.

The sensitivity for defect detection is highest when the lithographic pattern provides a uniform background for inspection; such is the case for the grating-like features that comprise the recording tracks for DTM, or the pillar arrays for BPM. Servo patterns generally have very different optical properties than the recording regions, which obscures the detection of defects in these regions. Figure 15a shows a portion of a specular-channel inspection of a DTR template. Servo patterns are evident as bright vertical stripes in the image, periodic in the theta direction of the disk scan. A pattern defect is indicated by the circle in the image. Figure 15b plots a line scan through this defect. If a simple threshold algorithm were applied to this data, it would not be possible to isolate the defect from the servo patterns. In Figure 15c, frequency filtering has been employed to attenuate the periodic signal associated with the servo pattern.[13] The defect signal has been amplified relative to a background signal, and it is now possible to apply a simple threshold algorithm to isolate the defect pixels, as seen in Figure 15d. This approach takes advantage of the rotational symmetry of PM patterns, and has proven to be effective for detection of defects embedded within servo patterns as well as in recording regions.

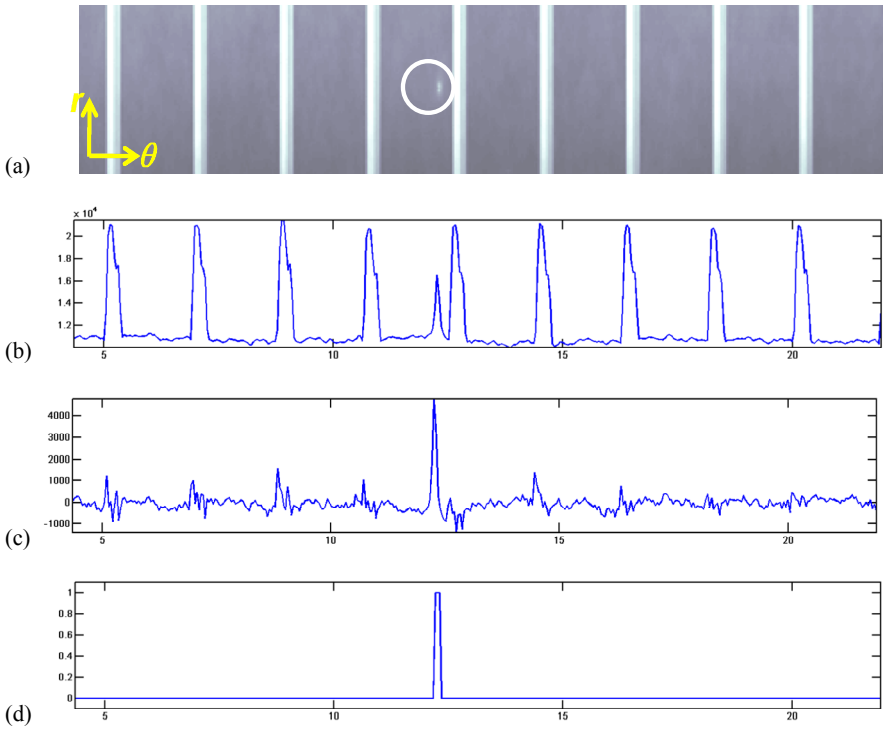

Figure 15. (a) Specular-channel Candela image of a DTR imprint template. Servo patterns are evident as vertical stripes, periodic in the theta direction. A pattern defect is indicated by the circle. (b) A line scan of the Candela image, passing through the defect. (c) Frequency filtering of the line scan data attenuates the periodic signal that is associated with the servo patterns. (d) A threshold function clearly identifies the defect pixels.

Downloaded from SPIE Digital Library on 23 Nov 2011 to 216.110.75.11. Terms of Use: http://spiedl.org/terms

b. Defect Analysis

Examples of defects seen on the template are shown in Figure 16. The most common defect type is missing patterns, as shown in Figure 16a. This type of defect shows up as a bright spot on a dark background. Particle type defects tend to be darker than the media background as shown in Figure 16b.

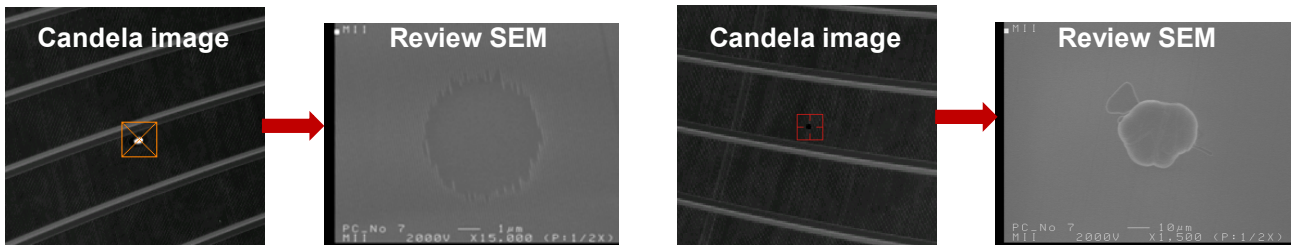

Figure 16. Defects detected with the Candela on a replica template. a) Missing patterns, b) particle on top of the pattern

Figure 17 displays the most common defects during the imprint process: particles and non-fill defects. Particle defects are the dominant defect and result primarily from insufficient cleaning of the disk. Non-fill defects are small in number relative to particle defects, and occur primarily from imperfections in the drop generation pattern. Small refinements to the software will further reduce this defect type.

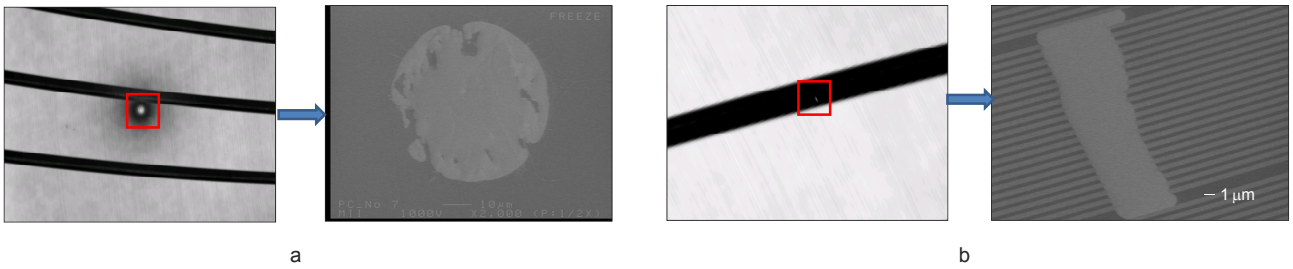

Figure 17. Imprint defects: a) Particle induced defect. b) Non-fill defect.

A run of two hundred disks was performed to monitor defectivity over the course of the run. Candela images of four of the disks are shown in Figure 18. Shown are the images from disks 10, 90, 130 and 200.

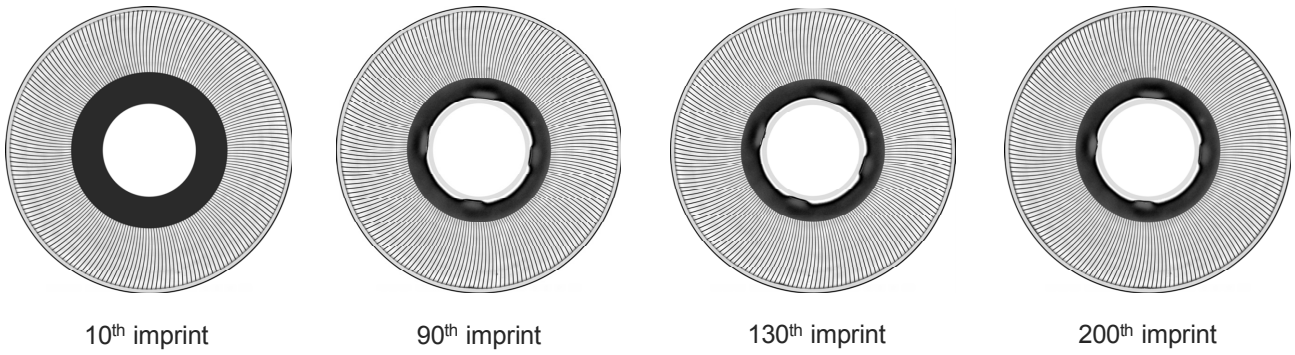

Figure 18. Candela images of four disks over a 200 disk run.

Downloaded from SPIE Digital Library on 23 Nov 2011 to 216.110.75.11. Terms of Use: http://spiedl.org/terms

The image files were collected and compared in a similar manner to what is routinely done in the semiconductor industry. Because align marks are included on every disk, it is possible to align the image files and compare defectivity from disk to disk. The results of this comparison are shown in Figure 19. Plotted is the total defect area ratio as a function of imprint number. The target for total defect area ration is 1e-4, and the data comes in well under this target. Defectivity does trend upwards, however, and is clearly dependent on the number of particle related defects. Improvements in disk cleaning are expected to mitigate the particle events and significantly extend the lifetime of the template.

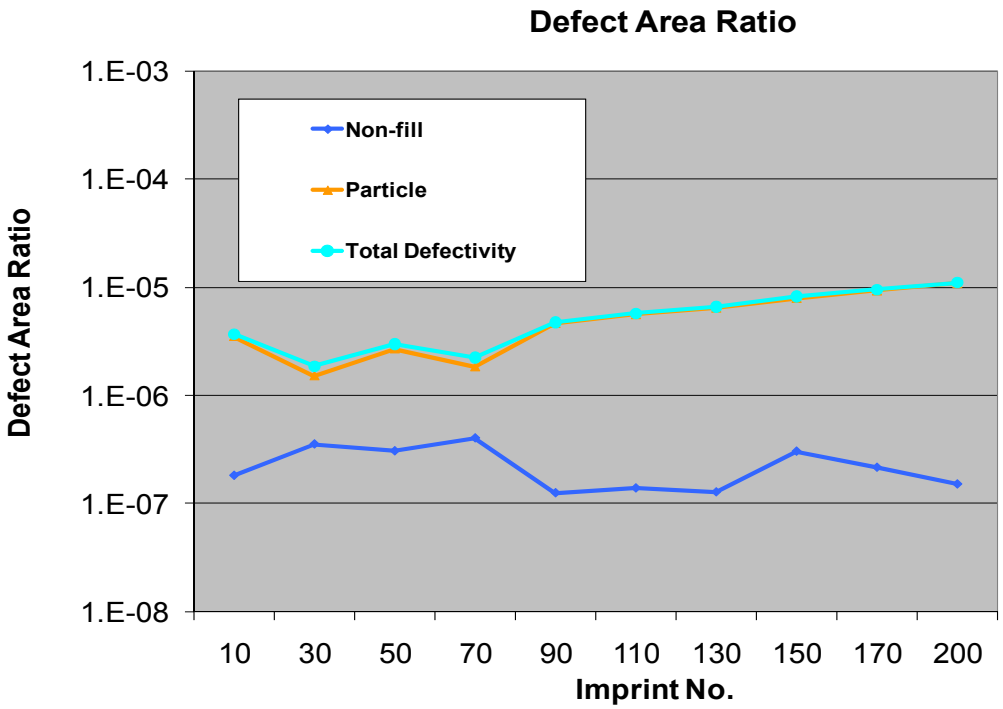

Figure 19. Defect area ratio as a function of imprint number. The total defectivity is well under the target of 1e-4.

Conclusions

Inspection of masks and low defectivity during imprinting are two key issues to be addressed for both the semiconductor and patterned media markets. In this work we have demonstrated the ability to inspect imprint masks with both electron beam and optical inspection tools. For the patterned media market, Candela systems have been used to inspect both wafers and disks. Defect levels are promising, and it is clear that the reduction of initial mask and template defects along with clean substrates will further reduce defectivity and extend mask/template life.

Acknowledgments

The authors would like to thank Masaaki Kurihara, Shiho Sasaki, Nobuhito Toyama and Naoya Hayashi from Dai Nippon Printing for their excellent imprint mask fabrication work. The authors are also grateful for the outstanding imaging results provided by Keizo Yamada and Osaumu Nawata from Holon Co., Ltd and by John Whittey from KLA-Tencor. Finally, the authors would like to express their gratitude to Mark McCord and Bo Magluyan from KLA-Tencor, and to Hong Xiao from Hermes Microvision for the exceptional results obtained on the e-beam wafer inspection systems.

Downloaded from SPIE Digital Library on 23 Nov 2011 to 216.110.75.11. Terms of Use: http://spiedl.org/terms

References

1. M. Colburn, S. Johnson, M. Stewart, S. Damle, T. Bailey, B. Choi, M. Wedlake, T. Michaelson, S. V. Sreenivasan, J. Ekerdt, and C. G. Willson, Proc. SPIE, Emerging Lithographic Technologies III, 379 (1999).
2. M. Colburn, T. Bailey, B. J. Choi, J. G. Ekerdt, S. V. Sreenivasan, Solid State Technology, 67, June 2001.
3. T. C. Bailey, D. J. Resnick, D. Mancini, K. J. Nordquist, W. J. Dauksher, E. Ainley, A. Talin, K. Gehoski, J. H. Baker, B. J. Choi, S. Johnson, M. Colburn, S. V. Sreenivasan, J. G. Ekerdt, and C. G. Willson, Microelectronic Engineering 61-62 (2002) 461-467.
4. R. S. Sasaki, T. Hiraka, J. Mizuochi, A. Fujii, Y. Sakai, T. Sutou, S. Yusa, K. Kuriyama, M. Sakaki, Y. Morikawa, H. Mohri, N. Hayashi, Proc. SPIE Vol. 7122, 71223P (2008).
5. S.V. Sreenivasan, P. Schumaker, B. Mokaberi-Nezhad, J. Choi, J. Perez, V. Truskett, F. Xu, X, Lu, presented at the SPIE Advanced Lithography Symposium, Conference 7271, 2009.
6. K. Selenidis, J. Maltabes, I. McMackin, J. Perez, W. Martin, D. J. Resnick, S.V. Sreenivasan, Proc. SPIE Vol. 6730, 67300F-1, 2007.
7. I. McMackin, J. Choi, P. Schumaker, V. Nguyen, F. Xu, E. Thompson, D. Babbs, S. V. Sreenivasan, M. Watts, and N. Schumaker, Proc. SPIE **5374**, 222 (2004).
8. L. Jeff Myron, L. Gershtein, G. Gottlieb, B. Burkhardt, A. Griffiths, D. Mellenthin, K. Rentzsch, S. MacDonald, G. Hughes, Proc. SPIE 5752, 384-391, (2005).
9. B.J. Choi, et al; SPIE Intl. Symp. Microlithography: Emerging Lithographic Technologies, 2001 Santa Clara, CA.
10. G. M. Schmid, C. Brooks, Z. Ye, S. Johnson, D. LaBrake, S. V. Sreenivasan, and D. J. Resnick, Proc. SPIE 7488, 748820 (2009).
11. H. Xiao, L. Ma, F. Wang, Y. Zhao, J. Jau, K. Selinidis, E. Thompson, S. V. Sreenivasan, and D. J. Resnick, Proc. SPIE 7488, 74881V (2009).
12. I. McMackin; J. Perez; K. Selinidis; J. Maltabes; D. Resnick; S. V. Sreenivasan, Proc. SPIE 6921, Emerging Lithographic Technologies XII, Frank M. Schellenberg, Editors, 69211L, 2008.
13. Schmid, G. M., N. Khusnatdinov, K. Luo, J. Fretwell, H. Wada, and D. Resnick, "Toward Automated Pattern Inspection and Defect Characterization for Patterned Media Lithography", presented at The 53rd International Conference on Electron, Ion, and Photon Beam Technology and Nanofabrication" on May 28, 2009.

Downloaded from SPIE Digital Library on 23 Nov 2011 to 216.110.75.11. Terms of Use: http://spiedl.org/terms